Article ID: 1007-4627(2016) 02-0122-09

Precision Mass Measurements of Short-lived Nuclides at the Heavy-ion Storage Ring in Lanzhou

ZHANG Yuhu(张玉虎)[1]，WANG Meng(王 猛)[1]，Yu. A. Litvinov[1,2]，XU Hushan(徐瑚珊)[1]

(*1. Key Laboratory of High Precision Nuclear Spectroscopy and Center for Nuclear Matter Science, Institute of Modern Physics, Chinese Academy of Sciences, Lanzhou 730000, China;*
2. GSI Helmholtzzentrum für Schwerionenforschung, Planckstraße 1, Darmstadt 64291, Germany)

Abstract: Recent commissioning of the Cooler Storage Ring at the Heavy Ion Research Facility in Lanzhou enabled us to conduct high-precision mass measurements at the Institute of Modern Physics in Lanzhou (IMP). In the past few years, mass measurements were performed using the CSRe-based isochronous mass spectrometry employing the fragmentation of the energetic beams of ^{58}Ni, ^{78}Kr, ^{86}Kr, and ^{112}Sn projectiles. Masses of short-lived nuclides on both sides of the stability valley were addressed. Relative mass precision of down to $10^{-6} \sim 10^{-7}$ is routinely achieved. The mass values were used as an input for dedicated nuclear structure and astrophysics studies, providing for instance new insights into the rp-process of nucleosynthesis in X-ray bursts. In this contribution, we briefly review the so far conducted experiments and the main achieved results, as well as outline the plans for future experiments.

Key words: storage ring; isochronous mass spectrometry; binding energy; isobaric multiplet mass equation; X-ray burst

CLC number: O571.21 **Document code:** A **DOI:** 10.11804/NuclPhysRev.33.02.122

1 Introduction

The mass is a fundamental property of atomic nucleus. The complex interplay of strong, weak and electromagnetic interactions in this many-body quantum system contributes to the difference between its mass and the sum of the masses of its free constituent nucleons. Precise and systematic measurements of nuclear masses not only provide indispensable information on nuclear structure, but also deliver important input data for applications in nuclear astrophysics[1–3]. Historically, the well-known shell structure and pairing correlations were discovered in stable nuclei via nuclear masses[4]. Similarly, new nuclear structure effects may be seen as irregularities on a generally smooth nuclear mass surface[5]. One of the present challenges in nuclear structure is to understand the shell evolution at extreme neutron-to-proton ratios, where the well-known magic numbers may disappear and the new shell closures may form[6–8].

About 7 000 nuclides are expected to exist in nature while masses of 2 438 nuclides are known experimentally[9]. The nuclides with still unknown masses lie far away from the valley of β-stability and are difficult to measure due to extremely low production cross sections and short lifetimes. Most of them are barely within reach of the present and will remain unaccessible at the next-generation radioactive beam facilities[10]. However, the interest to the new masses is huge[3], which is motivated, *e.g.*, by their need as an input in modelling explosive nucleosynthesis processes in stars[11–12]. For such calculations, the properties of unknown nuclei have to be estimated theoretically. However, accurate predictions of nuclear masses is still a big challenge for theories[13–14] and new masses are needed for their testing and constraining.

New mass measurements inevitably require very efficient and fast experimental techniques[15]. One such technique is the storage-ring mass spectrometry[16]. In this article we present a brief introduction

Received date: 21 Apr. 2016;

Foundation item: National Basic Research Program of China (973 Program)(2013CB834401); National Natural Science Foundation of China(U1232208, U1432125, 11205205, 11035007); Chinese Academy of Sciences, and Helmholtz-CAS Joint Research Group (HCJRG-108); Ministry of Science and Technology of China (Talent Young Scientist Program); China Postdoctoral Science Foundation (2014M562481); Western Light Talent Training Program of Chinese Academy of Sciences

Biography: ZHANG Yuhu(1962–), male, Gaoyi, Hebei, Professor, working on experimental nuclear physics; E-mail: yhzhang@impcas.ac.cn

to the facilities and the characteristic experiments performed in the Cooler Storage Ring at the Heavy Ion Research Facility in Lanzhou (HIRFL-CSR)[17]. Selected recent results and their impact for nuclear physics and astrophysics are reviewed. Planned technical developments and the envisioned future experiments are outlined.

2 Storage ring mass spectrometry

Storage ring mass spectrometry was pioneered at GSI in Darmstadt[18]. For an ion circulating in the storage ring, the revolution time, T, is related with its mass-over-charge ratio, m/q, via the following expression:

$$T = \frac{L}{c} \cdot \sqrt{1 + \left(\frac{mc}{q}\right)^2 \cdot \frac{1}{(B\rho)^2}} \ , \qquad (1)$$

where L is the orbit length of the ion, c the speed of light, and $B\rho$ the magnetic rigidity. Within a certain magnetic rigidity acceptance, $\Delta B\rho$, orbit lengths of ions are not constant. The relative time changes, $\Delta T/T$, are determined in the first order approximation by[18–20]:

$$\frac{\Delta T}{T} = \frac{1}{\gamma_t^2} \cdot \frac{\Delta(m/q)}{(m/q)} - \left(1 - \frac{\gamma^2}{\gamma_t^2}\right) \cdot \frac{\Delta v}{v} \ , \qquad (2)$$

where γ is the relativistic Lorentz factor, v the velocity of the ion. γ_t is the so-called transition energy of the ring[18] which connects the relative change of the orbit length to the relative change of magnetic rigidity of the circulating ions. In order to determine m/q-values of stored ions, revolution times of the ions need to be measured and the second term has to be made negligibly small. One way to achieve the latter is to use a special ion-optical setting of the ring and inject the ions with $\gamma = \gamma_t$. This is the basis of the isochronous mass spectrometry (IMS)[21–24]. In the IMS, the velocity spreads of the ions are compensated by the orbit lengths and their revolution times are a direct measure of m/q of the ions. The IMS is ideally suited for the mass measurement of short-lived nuclides[25].

3 Experimental details

HIRFL-CSR is an acceleration complex consisting of a separated-sector cyclotron (SSC, $K = 450$), and a main cooler-storage ring (CSRm) operating as a heavy-ion synchrotron. The CSRm has a circumference of 161 m and a maximum magnetic rigidity $B\rho$ of 10 Tm, and the $^{12}C^{6+}$ and $^{238}U^{72+}$ ions can be accelerated typically to about 1 GeV/u and 400 MeV/u, respectively. A detailed description of the HIRFL-CSR acceleration complex can be found in Refs. [17, 27]. The layout of the high energy part of the facility is illustrated in Fig. 1.

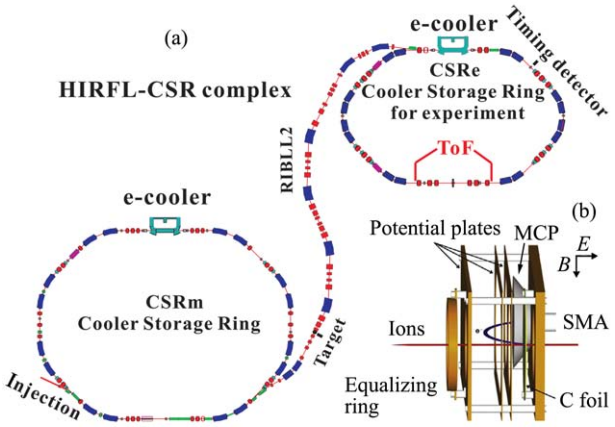

Fig. 1 (color online) (a) Layout of HIRFL-CSR complex at IMP including the synchrotron CSRm, the in-flight fragment separator RIBLL2, and the experimental storage ring CSRe[17], (b) Schematic view of the timing detector[29].

Accelerated in the main cooler-storage ring CSRm to typically 350 ∼ 480 MeV/u, stable ion beams are fast extracted and focused on a 10 ∼ 15 mm thick beryllium target placed in front of the in-flight fragment separator RIBLL2. The reaction products from projectile fragmentation are selected and analyzed by the RIBLL2 and a cocktail beam is injected into the CSRe[26]. The optical settings of the RIBBL2 and CSRe are tuned for the ion species of interest. All other nuclear species within the $B\rho$ acceptance of RIBLL2-CSRe of ±0.2% are transmitted and stored as well. The CSRe has a circumference of about 129 m and a maximal $B\rho = 8.4$ Tm[27]. It has two long straight sections. One of them is taken by an electron cooler device and two timing detectors (ToF) are being installed in the other one. The CSRe has $\gamma_t = 1.395$. In order to fulfill the IMS requirement, the primary beam energy has to be tuned such that the products of interest have $\gamma = \gamma_t = 1.395$ after the production target. About 10 ions are stored at each injection[28]. The revolution times are measured using a dedicated timing detector[29] (see Fig. 1). It is equipped with a 19 μg/cm^2 carbon foil of 40 mm in diameter. Secondary electrons are released from the foil surface due to ions passing through it. The electrons are guided isochronously by perpendicularly arranged electric (E) and magnetic (B) fields to a micro-channel plate (MCP) counter. The recording time is typically 200 μs corresponding to more than 300 revolutions of the ions in the ring. The detection efficiency varies from ∼ 20% to ∼ 70% depending on the charge and the number of stored ions[29], where the latter value is about the maximal one determined by the active surface of the MCP. For more details see Ref. [29]. The periodic timing signals are used to determine the revolution times of each individual ion.

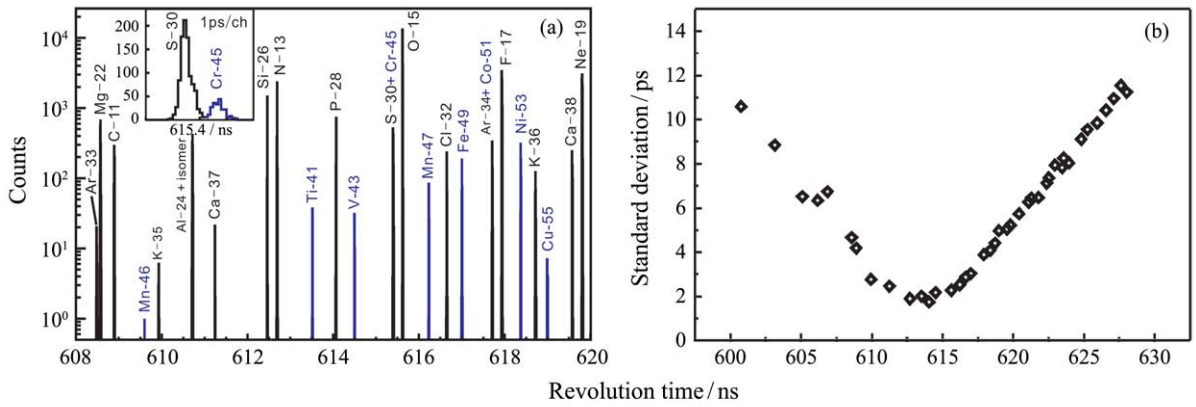

Fig. 2 (color online) (a) The revolution time spectrum of ^{58}Ni projectile fragments zoomed in at the time window of 608 ns $\leqslant t \leqslant$ 620 ns[30]. The insert shows the well-resolved peaks of $^{30}S^{16+}$ and $^{45}Cr^{24+}$ nuclei with very similar m/q values. Nuclei with masses determined in this experiment and those used as references are indicated with blue and black colour, respectively. (b) Standard deviations of the revolution time peaks for the full spectrum.

Measured revolution times of all ions comprise a revolution time spectrum. A part of the spectrum for ^{58}Ni projectile fragments is given in Fig. 2(a)[30]. Fig. 2(b) shows the peak widths as a function of the revolution time. The parabolic shape is due to the fact that the spectrum covers a broad range of m/q values of $\Delta(m/q)/(m/q) \sim 13\%$ while the condition $\gamma \approx \gamma_t$ is fulfilled in a limited region[16, 31]. The maximum mass resolving power reaches $m/\delta m = 180\,000$. Identification of the revolution time peaks is done by comparing the measured and a simulated spectra[22, 32–33].

In order to determine the m/q ratios, nuclides with well-known masses[9] are used to calibrate the revolution time spectrum. For this purpose a polynomial function of up to the third order[32] is used. The unknown m/q values are determined by interpolating or extrapolating with the fitted function. The details on the data analysis can be found in Refs. [30, 32, 34]. Up to now, no systematic errors had to be added in our analyses, which points to a good quality of the overall analysis procedure.

4 Experimental results

Several experiments have been conducted using ^{58}Ni, ^{78}Kr, ^{86}Kr, and ^{112}Sn primary beams. Fig. 3 shows a summary of masses measured. Typical relative mass uncertainties of $\delta m/m = 10^{-6} \sim 10^{-7}$ are achieved. Some of the results have been published in Refs. [28, 30, 32, 34–37] and the new mass values were included into the latest Atomic Mass Evaluation AME′12[9]. The data analysis for the neutron-deficient ^{112}Sn fragments and the $T_z = -2, -1$ pf-shell nuclides using ^{58}Ni beam are presently in progress. In the following, we present implications of our measurements with respect to nuclear structure and astrophysics applications.

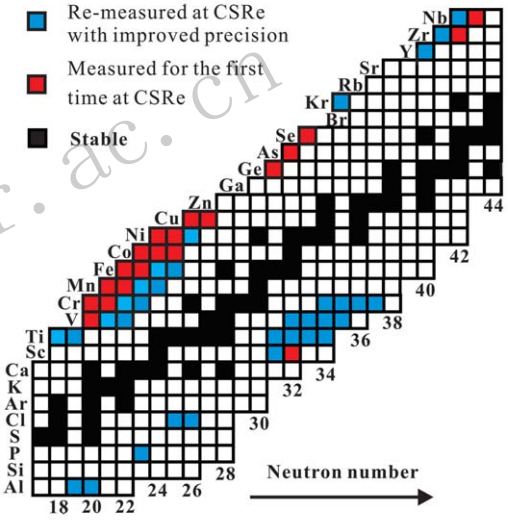

Fig. 3 (color online) The results of isochronous mass measurements performed at IMP (see Refs. [28,30,32,34-37]).

4.1 Masses of pf-shell nuclei and test of nuclear mass models

The masses of the $T = -2, -3/2, -1$ pf-shell nuclei have been measured using the IMS in CSRe (see Fig. 3). The highest precision of 5 keV for ^{54}Ni has been achieved corresponding to the relative uncertainty of $\delta m/m \sim 1 \times 10^{-7}$. These new results allowed us to test the accuracy and the predictive power of different mass models.

The accuracy of the current theoretical nuclear mass models have been recently investigated in Ref. [38]. Among the ten often-used models of various nature, the macroscopic-microscopic model of Wang and Liu[39–40], the latest version labeled as WS4[41], and the Duflo and Zuker (DZ28) mass model[42] are found to be more accurate in various mass regions with the smallest rms (root-mean square) values of

250 ∼ 500 keV. Their mass predictions are therefore compared with the experimental masses for the $T_z = -1$ nuclei in Fig. 4. We also plot the calculated results from the ETFSI-Q mass table[43]. One can see the prediction powers and accuracies of the models. We noticed that the differences between model predictions and the experimental masses, $ME_{\rm th} - ME_{\rm exp}$, show oscillations for all models. Only the WS4 model yields a regular zig-zag staggering around zero (see Fig. 4). This may indicate that both the nuclear pairing and the smooth A-dependence of nuclear masses have been more properly described in WS4 than in the other models, leading to more accurate description of the nuclear masses. Of course, the refined treatments of nuclear pairing are still needed in order to reduce the staggering.

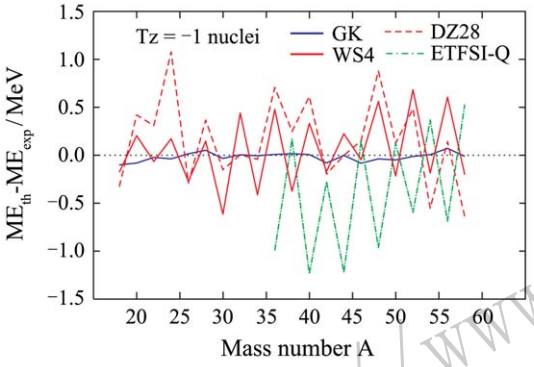

Fig. 4　(color online) Differences of the experimental mass excesses and the model prodictions for the $T_z = -1$ nuclei. Note that the GK mass relation gives more accurate mass predictions with respect to the mass models.

The masses of lighter neutron-deficient nuclei can be more precisely predicted by using the local mass relationships such as the well-known Garvey and Kelson[44] mass relation and the isobaric multiplet mass equation (IMME). The GK mass relation has been used here to predict the masses of $T_z = -1$ nuclei and compared with the experimental ones in Fig. 4. One see that the simple GK mass relation predicts more accurate masses than any mass model calculations, and the regular staggering in the model calculations has been nearly removed in the GK mass predictions.

4.2　Mass of ^{53}Ni and test of the Isobaric Multiplet Mass Equation

Measurements of neutron-deficient ^{58}Ni projectile fragments yielded new masses for ^{41}Ti, ^{43}V, ^{45}Cr, ^{47}Mn, ^{49}Fe, ^{51}Co, ^{53}Ni, and ^{55}Cu $T_z = -3/2$ nuclei[30, 35–36]. These new masses enabled us to test the validity of the isobaric multiplet mass equation (IMME) in the fp-shell nuclei[30, 45–46].

The IMME is based on the fundamental concept of the isospin symmetry in nuclear physics. It connects the members of an isobaric multiplet via[47–48]:

$$ME(A,T,T_z) = a(A,T) + b(A,T)\cdot T_z + c(A,T)\cdot T_z^2, \quad (3)$$

where a, b, and c are parameters depending on the atomic mass number A and the total isospin T, and $T_z = (N-Z)/2$. Extra terms such as $d\cdot T_z^3$ or $e\cdot T_z^4$ can be added to the IMME in order to provide a measure for any deviation from the quadratic form. Prior to our measurements, there have been extensive tests in the sd-shell nuclei (see Ref. [49] and references therein). However, no significant deviations were found except for slight disagreements at A =8, 9, 32, and 33. Our new masses and energies of the isobaric analog states in the $T_z = \pm 1/2$ nuclei[50–51] provide data for four $T = 3/2$ isospin quartets at $A = 41, 45, 49$, and 53. While for the former three quartets the data are in a reasonable agreement with the quadratic form of the IMME, there is a deviation for $A = 53$ isobaric multiplet, which can be quantified by adding a cubic term, $d\cdot T_z^3$. The d-coefficients for A = 41, 45, 49, and 53 are plotted in Fig. 5 together with recent results for the sd-shell nuclei[52–56]. The obtained $d = 39 \pm 11$ keV for $A = 53$ ($T = 3/2$) quartet deviates by 3.5σ from zero thus indicating a dramatic breakdown of the quadratic form of the IMME. We note that this rather large d coefficient cannot be explained by neither the existing nor new theoretical calculations of isospin mixing. For more details see Ref. [30].

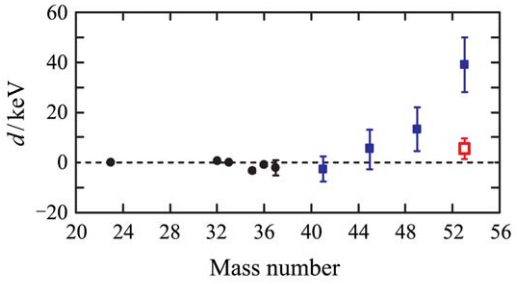

Fig. 5　(color online) d coefficients for the four $T = 3/2$ isobaric multiplets in pf-shell (squares). Experimental data since 2001 (circles)[52–56] are shown for comparison. The open red square is taken from the value in Ref. [57] which is obtained using the newly determined excitation energy of the $T = 3/2$ IAS in ^{53}Co.

The breakdown of IMME should be re-investigated by improved experimental data. From Eq. (3), the d coefficient is obtained as:

$$d = \frac{1}{6}\left\{\left[ME_{(+\frac{3}{2})} - ME_{(-\frac{3}{2})}\right] - 3\left[ME_{(+\frac{1}{2})} - ME_{(-\frac{1}{2})}\right]\right\}, \quad (4)$$

where the subscripts of the mass excesses stand for the isospin projection $T_z = (N-Z)/2$. The mass errors are

0.6 keV and 3.4 keV for ^{53}Mn and ^{53}Fe, it is very desirable to redetermine the masses of the $T=3/2$ states of ^{53}Ni and ^{53}Co within an uncertainty down to keV. More attention should be paid to the isobaric analog states in ^{53}Co and ^{53}Fe since the errors in the mass of the $T_z=\pm1/2$ members are three times as important as those in the $T_z=\pm3/2$ members (see Eq. (4)) for an evaluation of d and therefore in checking the validity of the IMME. Indeed, a recent experiment has been performed to redetermine the excitation energy of the $T=3/2$ IAS in ^{53}Co through the measurements of β-delayed γ transitions of ^{53}Ni[57]. It was found that the $T=3/2$ IAS in ^{53}Co is ∼70 keV below the previously assigned IAS on the basis of β-p emission data[51]. Using this new datum, the d coefficient can be calculated from Eq. (4) to be $d=5.4\pm4.6$ which is consistent with zero within 1.2σ (see Ref. [57] for details).

4.3 Mass of ^{65}As and waiting points on the path of rp-process of type I X-ray burst

Using the masses of ^{64}Ge[58] and ^{65}As[32, 34], the proton separation energy of ^{65}As has been determined to be $S_p(^{65}\mathrm{As})=-90(85)$ keV. Our result confirmed experimentally that ^{65}As is unbound against the proton emission at the 68.3% confidence level.

The new $S_p(^{65}\mathrm{As})$ value turned out to be important for the modelling of the rapid proton capture process (*rp*-process) in Type I X-ray bursts[59–61]. It has been long considered that ^{64}Ge, ^{68}Se, and ^{72}Kr nuclides are the major waiting-point nuclei along the path of the *rp*-process, since the stellar effective lifetimes of these waiting points depend exponentially on the S_p[60]. The $S_p(^{69}\mathrm{Br})$ and $S_p(^{73}\mathrm{Rb})$ are known to be negative from experiments indicating that both nuclides are fast proton emitters[62–63]. This makes it likely that ^{68}Se and ^{72}Kr are strong waiting points, although two-proton (2p) captures can somewhat reduce their effective lifetimes[60].

Due to its long half-life of $t_{1/2}=64(3)$ s [9] and since it is encountered first during the rp-process, the ^{64}Ge nucleus is considered to be the most important potential waiting point[61]. Before our measurement, only a model dependent lower limit of $S_p(^{65}\mathrm{As})>-250$ keV existed from the observation of the β^+-decay of ^{65}As[64]. Our new $S_p(^{65}\mathrm{As})$-value was used in one-zone X-ray burst model[65] calculations, which allowed us to define the temperatures and densities needed to bypass the ^{64}Ge waiting point.

Fig. 6(a) shows regions in the temperature-density plane where proton captures reduce the effective lifetime of ^{64}Ge to less than 50% of the β^+-decay lifetime thus resulting in a less effective waiting point. It can be seen that for densities below 2×10^5 g/cm^3 the required temperature range is rather narrow around 1.3 GK. For lower temperatures, ^{64}Ge can only be bypassed at higher densities. Varying our $S_p(^{65}\mathrm{As})$ value within 2σ provides essentially identical light curves [see Fig. 6(b)] demonstrating that our accuracy is sufficient to eliminate the effect of the ^{65}As mass uncertainty in X-ray burst calculations[34]. We find that 89% ∼ 90% of the reaction flow passes through ^{64}Ge via proton capture thus indicating that ^{64}Ge is not a significant rp-process waiting point. In contrast, using the estimated upper 2σ limit for ^{65}As from AME′03[66] ($S_p(^{65}\mathrm{As})\approx-650$ keV) leads to a reduction of the proton capture flow through ^{64}Ge to 54% with a significant effect on the calculated light curve as shown in the lower panel of Fig. 6.

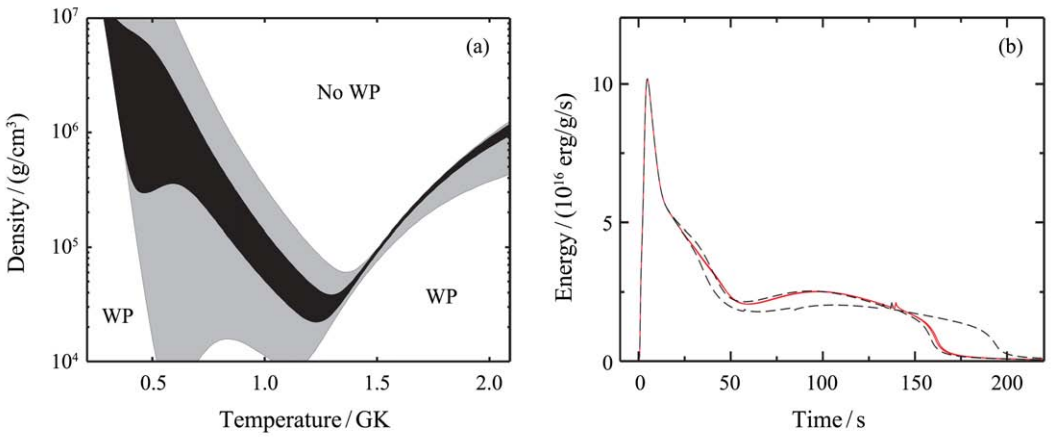

Fig. 6 (color online) (a) Regions in the temperature and density plane where ^{64}Ge is a strong waiting point (WP) with an effective lifetime longer than 50% of the β-decay lifetime. Shaded areas are deduced assuming 1σ variation of the AME′03[66] mass for ^{65}As (grey) and the ^{65}As mass from our work (black). (b) Calculated X-ray luminosity in a one zone X-ray burst model varying $S_p(^{65}\mathrm{As})$ within 2σ for masses from AME03 (dashed black lines) and from this work (solid red lines). Mode details can be found in Refs. [32,34].

4.4 Mass of ^{45}Cr and impact on the probable Ca-Sc cycle in the rp-process

Our experiments yielded a more precise mass excess $ME(^{45}\mathrm{Cr}) = -19515(35)$ keV [35] as compared to the previous value $ME(^{45}\mathrm{Cr}) = -18970(500)$ keV [66]. This resulted in an enhanced proton separation energy $S_p(^{45}\mathrm{Cr}) = (2.69 \pm 0.13)$ MeV instead of known before $S_p(^{45}\mathrm{Cr}) = (2.1 \pm 0.5)$ MeV. One-zone X-ray burst model calculations using the new $S_p(^{45}\mathrm{Cr})$ value enabled us to draw a conclusion on a possible formation of the so-called Ca-Sc cycle[67] in the rp-process.

The effect of the proton separation energy of ^{45}Cr on the rp-process path is illustrated in Fig. 7. ^{44}V and ^{43}Ti nuclei are in(p,γ) − (γ,p) equilibrium. The net proton capture flow at ^{43}Ti is determined by the leakage out of this equilibrium via the ^{44}V(p,γ)^{45}Cr reaction, the so-called 2p-capture process on ^{43}Ti[60]. For a low $S_\mathrm{p}(^{45}\mathrm{Cr})$ value allowed by the 3σ uncertainties of the AME'03 data[66], the ^{45}Cr(γ, p)^{44}V reaction becomes effective. This reduces the proton capture flow at ^{43}Ti leading to a significant β^+-decay branch in ^{43}Ti, which drives the reaction flow into ^{43}Sc, and then via a large (p,α) branch into ^{40}Ca. This Ca-Sc cycle limits strongly the reaction flow towards heavier elements and affects significantly the X-ray burst observables[67]. Fig. 7(a) shows the integrated reaction flow in the Ca-Sc cycle as a function of $S_p(^{45}\mathrm{Cr})$. Up to a proton separation energy of about 2 MeV, a strong cyclic reaction flow occurs. The extrapolated ^{45}Cr mass from AME′03 allows for a strong cycle which introduces a significant uncertainty in X-ray burst models. Our new $S_p(^{45}\mathrm{Cr})$ value basically excludes the formation of a significant cycle and therefore removes this uncertainty[35].

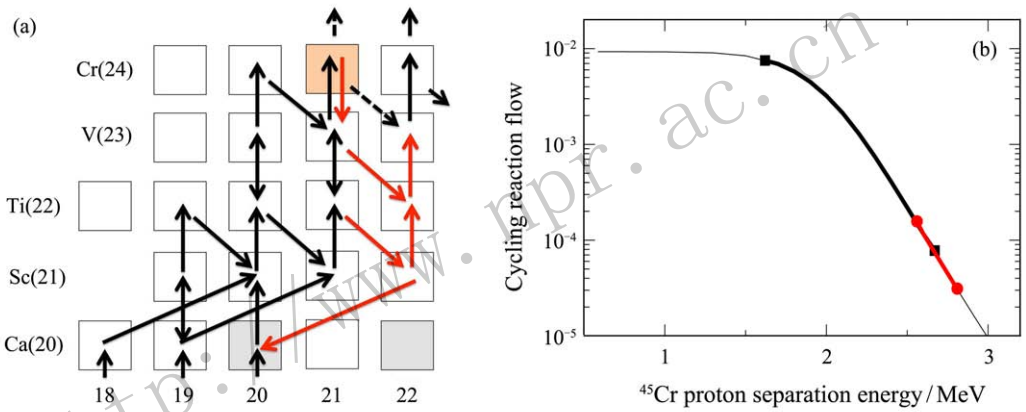

Fig. 7 (color online) (a) Integrated reaction flow in the Ca-Cr region during rp-process in X-ray bursts. Black arrows show the reaction flow for our new $S_p(^{45}\mathrm{Cr})$, while the red arrows indicate the reaction flow for a low $S_p(^{45}\mathrm{Cr})$ value from AME'03 [66]. Flows that disappear for the latter case are indicated as black dashed arrows. (b) Integrated reaction flow through the Ca-Sc cycle during an X-ray burst as a function of $S_p(^{45}\mathrm{Cr})$. The graph spans the 3σ uncertainty of $S_p(^{45}\mathrm{Cr})$ value from AME'03. The thick black line limited by filled squares indicates the 1σ uncertainty of $S_p(^{45}\mathrm{Cr})$ in AME'03, while the thick red line limited by filled circles indicates the 1σ uncertainty when using our new experimental result. For more details see Ref. [35].

4.5 Masses of neutron-deficient Y, Nb, and Zr isotopes and impact on the reaction path of rp-process to heavier mass region

Recent mass measurements of neutron-deficient ^{112}Sn projectile fragments yielded new masses for ^{79}Y, ^{81}Zr, ^{82}Zr, ^{83}Nb, and ^{84}Nb among which the masses of ^{82}Zr and ^{84}Nb were obtained for the first time up to a precision of $\sim$15 keV. These new masses allow us to deduce their proton and alpha separation energies (see Fig. 8) which are the important nuclear physics inputs for X-ray burst model calculations[68–69].

Our masses lead to the new experimental S_p-values for six nuclides along the reaction path of rp-process. Of particular interest is the significant reduction of S_p-values for ^{79}Y, ^{83}Nb (up to 500 $\sim$ 600 keV), and ^{81}Zr, ^{85}Mo (up to 800 $\sim$ 900 keV) compared to their values used in the previous model calculations[68–69]. The upper panel of Fig. 8 shows the systematics of S_p-values for some odd-Z even-N nuclides. One sees that S_p becomes more regular as a function of Z or N if our new values of ^{79}Y, ^{83}Nb are adopted. We note that model calculations have been performed in Ref. [69]; the authors call for precision mass measurements of ^{83}Nb, ^{86}Nb, and ^{86}Tc in order to refine the related theoretical rate calculations. In this sense, our work may contribute to this issue of nuclear astrophysis, that is presently in progress.

Another important issue is concerned with the existence of a Zr-Nb cycle in the rp-process due

to an island of very low α-separation energies for neutron-deficient Mo isotopes[60]. The low S_α-values are believed to induce the large ^{84}Mo$(\gamma,\alpha)^{80}$Zr or ^{83}Nb(p,α)^{80}Zr reaction rates that could terminate the rp-process to heavier mass region. A sudden drop of S_α-values, starting from ^{85}Mo and ^{87}Tc [see Ref. [68] and Fig. 8(b)], have been revealed on the basis of precision mass measurements of ^{85}Mo and ^{87}Tc[68]. However, the masses of ^{81}Zr and ^{83}Nb had a large uncertainty at the time being, the low α-separation energies for ^{85}Mo and ^{87}Tc [68] could be caused by this uncertainty. Using our newly measured masses of ^{81}Zr and ^{83}Nb, the α separation energies are 2.478(94) and 2.558(151) MeV, instead of 1538(165) and 1.704(300) MeV, for ^{85}Mo and ^{87}Tc, respectively. The new S_α values show no sudden drop at ^{85}Mo and ^{87}Tc [see the Fig. 8(b)]. This indicates that there might be no expected island of very low S_α-values for neutron-deficient Mo isotopes[60], and consequently, the *rp*-process in the X-ray bursts can continue to heavier Sn-Te mass region[65].

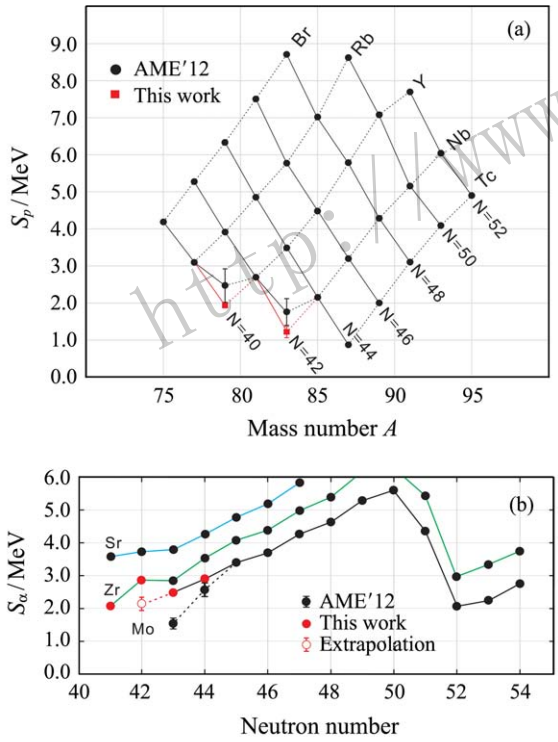

Fig. 8 (color online) (a) Proton separation energies (S_p) of nuclides with odd Z and even N according to AME′12 and our results. (b) Alpha separation energies S_α of Sr, Zr, and Mo isotopes from AME′12 and our results.

5 Summary and outlook

In the last years at HIRFL-CSRe we have successfully established the research program on direct mass measurements by employing the isochronous mass spectrometry (IMS). In this review we presented a few examples of obtained results that turned to be important for nuclear structure and astrophysics investigations[30, 34–36, 70–72]. Data of more experiments are being presently analysed.

Future experiments inevitably require improvements of the accelerator performance as well as measurement and analysis techniques. Recent technical developments at the CSRe can be found, *e.g.*, in Refs. [36, 73–75]. As shown in Fig. 2(b), a high resolving power of the IMS is achieved in a small range of revolution times. An additional information on the velocity or magnetic rigidity of each ion can be used to correct for non-isochronicity effects[31]. A proof-of-principle experiment was performed at GSI by restricting the acceptance to $\Delta B\rho/B\rho \sim 10^{-4}$[76]. In the case of the CSRe, two time-of-flight detectors were recently installed in the straight section of the CSRe. They will enable the in-ring measurement of the velocity of each stored ion without limiting the transmission. In turn this should allow us to improve the resolving power over the entire revolution time spectrum.

An essential development is also the commissioning of the time-resolved Schottky Mass Spectrometry (SMS)[77–79] in the CSRe. In addition to accurate mass measurements, SMS will enable a wide range of unique experiments with stored stable as well as radioactive highly-charged ions[79–80]. Furthermore, a new resonant Schottky pick-up, which allows for non-destructive frequency as well as intensity measurements of stored ions, has been developed[81]. A similar detector was now also installed in the CSRe[82]. Owing to a broad dynamic range, this detector is being capable of measuring frequencies of single stored ions as well as high intensity beams of several mA. Possibly, such detectors can replace in the future the time-of-flight detectors in IMS measurements. The intensity measurements will enable studies of radioactive decays of highly-charged ions as, *e.g.*, the studies of β-decay which could up to now be performed only at the ESR[79–80]. Also other nuclear physics experiments like for instance the studies of nuclear isomers, measurements of β-delayed neutron emission, proton- and α-capture reactions for nuclear astrophysics, in-ring nuclear reactions studies, and di-electronic recombination on exotic nuclei will be pursued in the future[83–85].

The multidisciplinary research program which is being developed at the CSRe, will be continued and further extended at the new-generation storage ring complex HIAF (High Intensity Accelerator Facility)[86]. HIAF is now in its planning phase and

shall offer complementary research opportunities for storage ring physics as compared to the corresponding programs at GSI/FAIR storage rings[79, 87–88], RARE RI-RING in RIKEN[89], and TSR@ISOLDE[90] in CERN.

Acknowledgments This review is based on the previous publications and some new unpublished data of our colleagues from the international collaboration performing experiments at HIRFL-CSR facility. To all of them we are deeply obliged. K.B. acknowledge support by the Nuclear Astrophysics Virtual Institute (NAVI) of the Helmholtz Association.

References:

[1] BLAUM K. Phys Rep, 2006, **425**: 1.
[2] LUNNEY D, PEARSON J M, THIBAULT C, *et al.* Rev Mod Phys, 2003, **75**: 1021.
[3] BLAUM K, LITVINOV YU A. Int J Mass Spectr, 2003, **349-350**: 1.
[4] BOHR A , MOTTELSON B R. Nuclear Structure, (Singapore: World Scientific Publishing),1998.
[5] NOVIKOV YU N, ATTALLAH F, BOSCH F, *et al.* Nucl Phys A, 2002, **697**: 92.
[6] KANUNGO R, NOCIFORO C, PROCHAZKA A, *et al.* Phys Rev Lett, 2009, **102**: 152501.
[7] KANUNGO R. Phys Scr T, 2013, **152**: 014002.
[8] OTSUKA T. Phys Scr T, 2013, **152**: 016007.
[9] AUDI G, KONDEV F G, WANG M *et al.* Chin Phys C, 2012 **36**: 1287.
[10] KURCEWICZ J, FARINON F, GEISSEL H,*et al.* Phys Lett B, 2012, **717**: 371.
[11] BERTULANI C A , GADE A. Phys Rep, 2010,**485**: 195.
[12] LANGANKE K, SCHATZ H, Phys Scr T, 2013, **152**: 014011.
[13] SOBICZEWSKI A, LITVINOV YU A. Phys Rev C, 2014, **89**: 024311.
[14] SOBICZEWSKI A, LITVINOV YU A. Phys Rev C, 2014 **90** 017302.
[15] BLAUM K, BLOCK M, CAKIRLI R B, *et al.* J Phys Conf Series, 2011, **312**: 092001.
[16] LITVINOV YU A, GEISSEL H, KNOBEL R, *et al.* Acta Phys Pol B, 2010, **41**: 511.
[17] ZHAN W L, XU H S, XIAO G Q, *et al.* Nucl Phys A, 2010, **834**: 694c.
[18] FRANZKE B, GEISSEL H, MÜNZENBERG G, *et al.* Mass Spectrometry Rev, 2008, **27**: 428.
[19] RADON T, KERSCHER TH, SCHLITT B, *et al.* Phys Rev Lett, 1997, **78**: 4701.
[20] RADON T, GEISSEL H, MÜNZENBERG G, *et al.* Nucl Phys A, 2000, **677**: 75.
[21] HAUSMANN M, ATTALLAH F, BECKERT K, *et al.* Nucl Instr Meth A, 2000, **446**: 569.
[22] HAUSMANN M, STADLMANN J, ATTALLAH F, *et al.* Hyperfine Interactions, 2001, **132**: 289.
[23] STADLMANN J. Phys Lett B, 2004, **586**: 27.
[24] SUN B, KNOBEL R, LITVINOV YU A, *et al.* Nucl Phys A, 2008, **812**: 1.
[25] GEISSEL H, LITVINOV YU A, ATTALLAH F, *et al.* Nucl Phys A, 2004, **746**: 150c.
[26] MEI B, XU H S, TU X L, *et al.* Phys Rev C, 2014, **89**: 054612.
[27] XIA J W, ZHAN W L, WEI B W, *et al.* Nucl Instr Meth A, 2002, **488**: 11.
[28] XU Hushan, ZHANG Yuhu, LITVINOV YU A, *et al.* Int J Mass Spectr, 2013, **349-350**: 162.
[29] MEI B, *et al.* Nucl Instr Meth in Phys Res Sect A, 2010, **624**: 109.
[30] ZHANG Y H, XU H S, LITVINOV YU A, *et al.* Phys Rev Lett, 2012, **109**: 102501.
[31] GEISSEL H, LITVINOV YU A. J Phys G, 2005, **31**: S1779.
[32] TU X L, WANG M, LITVINOV YU A, *et al.* Nucl Instr Meth A, 2011 **654**: 213.
[33] SUN B H, GEISSEL H, HAUSMANN M, *et al.* Chin Phys C, 2009, **33** (Suppl. 1): 161.
[34] TU X L, XU H S, WANG M, *et al.* Phys Rev Lett, 2011, **106**: 112501.
[35] YAN X L, XU H S, LITVINOV YU A, *et al.* Astrophys J Lett, 2013, **766**: L8.
[36] SHUAI P, XU H S, TU X L, *et al.* Phys Lett B, 2014, **735**: 327.
[37] XU X,WANG M, ZHANG Y H, *et al.* Chin Phys C, 2015, **39**: 104001.
[38] SOBICZEWSKI A, LITVINOV YU A. Phys Rev C, 2014, **89**: 024311.
[39] LIU M, WANG N, DENG Y, *et al.* Phys Rev C, 2011, **84**: 014333.
[40] WANG N, LIU M. Phys Rev C, 2011, **84**: 051303(R).
[41] WANG N, LIU M, WU X, *et al.* Phys Lett B, 2014, **734**: 215.
[42] DUFLO J, ZUKER A P. Phys Rev C, 1995, **52**: R23.
[43] PEARSON J M, NAYAKA R C, GORIELY S. Phys Lett B, 1996, **387**: 455.
[44] GARVEY G T, KELSON I. Phys Rev Lett, 1966, **16**: 197.
[45] ZHANG Y H, XU H S, LITVINOV YU A, *et al.* J Phys Conf Series, 2013, **420**: 012054.
[46] TU X L, Y SUN, Y H ZHANG, *et al.* J Phys G, 2014, **41**: 025104.
[47] WIGNER E P, PROC R A. Welch Found Conf on Chem Res. (Houston 1957) R.A. Welch Foundation.
[48] WEINBERG S, TREIMAN S B. Phys Rev, 1959, **116**: 465.
[49] LAM Y H, BLANK B, SMIRNOVA N A, *et al.* At Data Nucl Data Tables, 2013, **99**: 680.
[50] ANTONY M S, PAPE A, BRITZ J. At Data Nucl Data Tables, 1997, **66**: 1.
[51] DOSSAT C, N. ADIMI, F. AKSOUH, *et al.* Nucl Phys A, 2007, **792**: 18.
[52] PYLE M C, GARCíA A, TATAR E, *et al.* Phys Rev Lett, 2002, **88**: 122501.
[53] RINGLE R, SUN T, BOLLEN G, *et al.* Phys Rev C, 2007, **75**: 055503.

[54] YAZIDJIAN C, AUDI G, BECK D, *et al*. Phys Rev C, 2007, **76**: 024308.
[55] SAASTAMOINEN A, ERONEN T, JOKINEN A,*et al*. Phys Rev C, 2009, **80**: 044330.
[56] KANKAINEN A, T. ERONEN, D. GORELOV, *et al*. Phys Rev C, 2010, **82**: 052501.
[57] SU J, LIU W P, ZHANG N T, *et al*. Phys Lett B, 2016, **756**: 323.
[58] SCHURY P, BACHELET C, BLOCK M, *et al*. Phys Rev C, 2007, **75**: 055801.
[59] WALLACE R K, WOOSLEY S E. Astrophys J Suppl Ser, 1981, **45**: 389.
[60] SCHATZ H, APRAHAMIAN A, GÖRRES J, *et al*. Phys Rep, 1998, **294**: 167.
[61] PARIKH A, J. JOSÉ, ILIADIS C, *et al*. Phys Rev C, 2009, **79**: 045802.
[62] BLANK B, ANDRIAMONJE S, CZAJKOWSKI S, *et al*. Phys Rev Lett, 1995, **74**: 4611.
[63] JOKINEN A, OINONEN M. J. Ayst, *et al*. Z Phys, 1996, **355**: 227.
[64] WINGER J A, BAZIN D P, BENENSON W, *et al*. Phys Rev C, 1993, **48**: 3097.
[65] SCHATZ H, APRAHAMIAN A, BARNARD V, *et al*. Phys Rev Lett, 2001, **86**: 3471.
[66] AUDI G, WAPSTRA A H, THIBAULT C, *et al*. Nucl Phys A, 2003, **729**: 337.
[67] VAN WORMER L, GORRES J, ILIADIS C. *et al*. Astrophys J, 1994, **432**: 326.
[68] HAETTNER E, ACKERMANN D, AUDI G, *et al*. Phys Rev Lett, 2013, **106**: 122501.
[69] PARIKH A, JOSÉ J, SEITENZAHL I R, *et al*. Prog Part Nucl Phys, 2013, **69**: 225.
[70] WALKER P M. Nature Phys, 2013, **7**: 281.
[71] MARTINEZ-PINEDO G. Physik J, 2011, **10**: 16.
[72] SUN Y. Chin Sci Bull, 2011, **56**: 1637.
[73] ZHANG W, TU X L, WANG M, *et al*. Nucl Instr Meth A, 2014, **755**: 38.
[74] ZHANG W, TU X L, WANG M, *et al*. Nucl Instr Meth A, 2014, **756**: 1.
[75] GAO X, YUAN Y J, J C YANG, *et al*. Nucl Instr Meth A, 2014, **763**: 53.
[76] GEISSEL H, KNOÖBEL R, LITVINOV YU A, *et al*. Hyperfine Interactions, 2006, **173**: 49.
[77] LITVINOV YU A, GEISSEL H, NOVIKOV YU N, *et al*. Nucl Phys A, 2004, **734**: 473.
[78] LITVINOV YU A, GEISSEL H, RADON T, *et al*. Nucl Phys A, 2005, **756**: 3.
[79] LITVINOV YU A, BOSCH F. *et al*. Rep Prog Phys, 2011, **74**: 016301.
[80] BOSCH F, LITVINOV YU A, TH STOHLKER. Prog Part Nucl Phys, 2013, **73**: 84.
[81] NOLDEN F, HÜLSMANN P, LITVINOV YU A, *et al*. Nucl Instr Meth in Phys Res Sect A, 2013, **659**: 69.
[82] ZANG Y D, WU J X, ZHAO T C, *et al*. Chin Phys C, 2011, **35**: 1124.
[83] CHEN L X, WALKER P M, GEISSEL H, *et al*. Phys Rev Lett, 2013, **110**: 122502.
[84] ZHONG Q, AUMANN T, BISHOP S, *et al*. J Phys Conf Series, 2010, **202**: 012011.
[85] LITVINOV YU A, BISHOP S, BLAUM K, *et al*. Nucl Instr Meth B, 2013, **317**: 603.
[86] YANG J C. Nucl Instr Meth B, 2013, **317**: 179.
[87] STÖHLKER TH. Hyperfine Interact, 2014, **227**: 45.
[88] WALKER P M, LITVINOV YU A, H. GEISSEL. Int J Mass Spectr, 2013, **349-350**: 247.
[89] YAMAGUCHI T, YAMAGUCHI Y, OZAWA A. Int J Mass Spectr, 2013, **349-350**: 240.
[90] GRIESER M, LITVINOV YU A,RAABE R, *et al*. Eur Phys J Special Topics, 2012, **207**: 1.